

Auger-process-induced charge separation in semiconductor nanocrystals

Victor I. Klimov* and Duncan W. McBranch

Chemical Sciences and Technology Division, Los Alamos National Laboratory, Los Alamos, New Mexico 87544

(Received 20 November 1996)

Femtosecond nonlinear transmission techniques are applied to study mechanisms for optical nonlinearities and ultrafast carrier dynamics in CdS nanocrystals (NC's). The obtained data indicate the change in a dominant hole relaxation channel at high pump levels where nonlinear recombination effects start to play a significant role. This is manifested as a distinct difference in nonlinear-optical responses measured at low and high pump intensities in quasiequilibrium at long times after excitation. The analysis of the wavelength and time dependence of the nonlinear transmission over a wide pump-intensity range shows clearly that this difference is due to an Auger-process-assisted trapping of holes at surface/interface-related states. This trapping leads to efficient charge separation and the generation of a dc electric field that modifies the nonlinear optical response in NC's at high pump intensities. [S0163-1829(97)02620-9]

I. INTRODUCTION

Due to three-dimensional carrier confinement and a large surface-to-volume ratio, semiconductor nanocrystals (NC's) exhibit a number of interesting physical properties, not observable in bulk semiconductors (see, e.g., reviews in Refs. 1 and 2). Apart from interesting physics and chemistry, NC materials have attracted substantial recent interest for their potential in device applications, which can benefit from size-controlled spectral tunability, enhancement of the oscillator strength, and ultrafast relaxation dynamics, being largely controlled by the condition of the NC surface. Applications of NC materials in laser emitters,³ electroluminescent devices,⁴ switching elements,⁵ and solar batteries⁶ have been reported recently in the literature.

Extensive experimental and theoretical work has been done on NC's formed from II-VI semiconductors such as CdS, CdSe, and CdS_xSe_{1-x}. Different methods of preparation have been developed to synthesize the II-VI NC's with narrow-size distributions in both colloidal⁷ and solid-state forms.⁸ Theoretical description of the electronic structures in NC's has advanced from simple particle-in-the-box models⁹ to much more sophisticated approaches including finite-well and image-charge effects,¹⁰⁻¹² Coulomb interaction,¹³⁻¹⁵ nonparabolicity of the conduction band,^{16,17} and confinement-induced mixing of valence subbands.^{14,17,18} Semiconductor NC's exhibit large and fast optical nonlinearities that are dominated by a state filling^{19,20} with contributions from a number of less pronounced effects, such as a two-electron-hole pair interaction,^{21,22} trapped-carrier-induced dc Stark effect,²³ and excited-state absorption due to intraband transitions.²⁴

The nonlinear optical and luminescent properties of NC's are significantly affected by carrier dynamics. Carrier trapping (localization^{25,26}) and a nonradiative Auger process²⁷ are believed to play a major role in the early stages of carrier relaxation, resulting in ultrafast dynamics measured in femtosecond pump-probe, photoluminescence (PL) up-conversion, and photon-echo experiments.²⁵⁻²⁷ The mechanisms for carrier localization, and in particular the role of the surface/interface states, in the trapping process have not yet

been clarified. In two recent papers^{25,28} we reported studies of carrier dynamics in CdS NC's performed in the low-pump-intensity range where carrier relaxation was dominated by localization processes. Applying two complementary time-resolved techniques (femtosecond PL up-conversion and nonlinear transmission measurements), we observed separately the electron and hole relaxation paths. In particular, we have demonstrated that the hole is trapped into a localized state with a time constant ~ 1 ps, while the electron trapping occurs on a slower time scale of tens of picoseconds.

In the present paper we extend the pump-intensity range up to levels where nonlinear recombination effects start to play a significant role. The resulting data clearly indicate that hole relaxation channels are distinctly different at low and high pump levels, leading to a strong difference in optical nonlinearities observed in quasiequilibrium at long times after excitation. Experimental data and modeling show that this difference is due to an Auger-process-assisted trapping of the hole at surface/interface states that leads to efficient charge separation and generation of a dc electric field, which modifies the nonlinear optical response at high pump levels.

II. EXPERIMENT

CdS NC's of ~ 4 nm radius were grown in a glass matrix by a secondary heat treatment method.²⁹ In the present studies, we used the same samples as those described in Ref. 25. This allows a direct comparison of previously reported PL data²⁵ with nonlinear transmission results from the present paper.

Time-resolved nonlinear transmission was measured using a femtosecond pump-probe experiment. The samples were excited at 3.1 eV by frequency-doubled pulses from a regeneratively amplified mode-locked Ti-sapphire laser (Clark-MXR NJA-4/CPA-1000). The pulse duration is 100 fs, the maximum pulse energy is 1 mJ, and the repetition rate is 1 kHz. The transmission of the excited sample is probed by delayed pulses of a femtosecond continuum generated in a 1-mm-thick sapphire plate. As a measure of transmission changes we use the differential transmission (DT) defined as follows: $D = (T - T_0)/T_0 = \Delta T/T_0$, where T_0 and T are trans-

missions in the absence and in the presence of the pump, respectively. Pump-induced absorption changes ($\Delta\alpha$) can be derived from DT using the expression $\Delta\alpha d = -\ln(D+1)$ (d is the sample thickness), which reduces to $\Delta\alpha d \approx -D$ in the small-signal limit ($D \ll 1$).

Time-resolved DT was measured in two complementary experimental setups. DT spectra at a fixed delay time Δt between pump and probe pulses were recorded with a 0.15-m spectrometer coupled to a liquid-nitrogen-cooled charge coupled device by averaging the signal over 1000–2000 pulses. This type of measurement provides information on the spectral distribution of the nonlinear optical response over a broad spectral range (0.45–1.1 μm) with an accuracy up to 10^{-3} in DT. Single-wavelength DT dynamics were monitored with much higher accuracy using phase-sensitive detection, synchronized to the mechanically chopped pump beam. In this setup, reference and signal pulses are coupled to a monochromator followed by two large area p - i - n photodiodes. The signals from the photodiodes are differentially amplified and finally detected with a lock-in amplifier. The phase-sensitive technique has a detection limit for DT of 10^{-4} – 10^{-5} . All measurements reported below were performed at room temperature.

III. DIFFERENTIAL TRANSMISSION SPECTRA

First we examine time-resolved DT at low pump fluences $w_p < 0.5 \text{ mJ cm}^{-2}$, where the PL and DT dynamics are independent of the pump intensity. This presumably corresponds to excitation of less than one electron-hole (e - h) pair per NC on average and allows us to avoid the saturation of trap states and fast Auger recombination. DT spectra recorded in this pump range are shown in Figs. 1(a) and 1(b). At early times after excitation, the DT spectra are dominated by an intense bleaching band at 2.63 eV arising from state-filling-induced saturation of the lowest optical transition [$1S(e)$ - $1S_{3/2}(h)$] between electron and hole quantized states (for notation of quantum-confined states and optical transitions in NC's see, e.g., Ref. 17). As discussed in detail in Refs. 25 and 28, the initial stage of carrier relaxation in CdS NC's (during the first few picoseconds after excitation) is dominated by hole trapping with a very short time constant of about 1 ps. Due to a large difference between electron and hole masses in CdS ($m_h/m_e \sim 6$), the hole levels are more closely spaced than the electron levels. Therefore, at room temperature, the occupation number of the lowest $1S$ -electron state is significantly larger than that of the lowest $1S$ -hole state, meaning that the state-filling-induced bleaching of the lowest transition is dominated by the electron contribution.^{30,31} Therefore, the fast initial hole dynamics are not discernible in DT, but are well manifested in time-resolved PL as a rapid decay of the PL band at 2.63 eV and a shift of the PL maximum down to 2.56 eV that corresponds to the peak of the cw band-edge emission.^{25,28} This behavior has been explained by hole trapping at a shallow trap located 70 meV below the lowest hole quantized state. The transition coupling this state to the lowest electron quantized state dominates the cw band-edge PL. The DT dynamics presented in Fig. 1(a) are much slower than the PL dynamics for the same pump intensities.²⁵ The DT decay at 2.63 eV (the lowest optical transition between quantized states) is almost exponential with a time constant

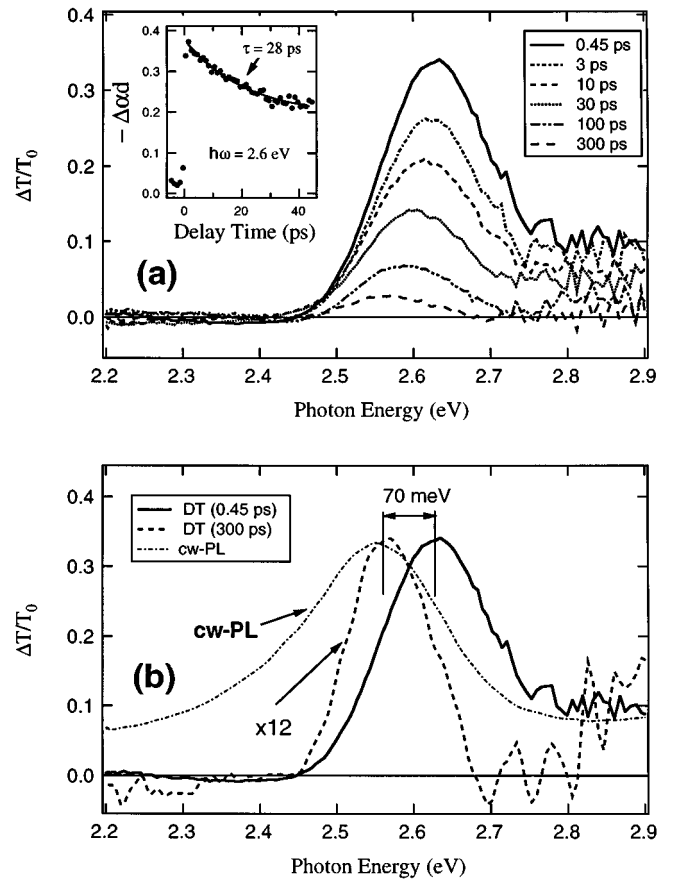


FIG. 1. (a) DT spectra recorded at different delay times after excitation at a pump level $w_p = 0.45 \text{ mJ cm}^{-2}$, below the threshold for nonlinear recombination processes. The inset shows the DT time evolution recorded at the same pump level at $\hbar\omega = 2.6 \text{ eV}$ (circles), along with a fit to an exponential decay (solid line). (b) Normalized DT spectra measured at $\Delta t = 0.45 \text{ ps}$ (solid line) and 300 ps (dashed line) ($w_p = 0.45 \text{ mJ cm}^{-2}$) in comparison to the cw PL spectrum.

of about 30 ps [see the inset to Fig. 1(a)]. This decay can be explained by electron trapping at a deep state that is involved in the long-lived deep-trap emission located at $\sim 1.9 \text{ eV}$.²⁸ This explanation is in agreement with direct measurements of buildup dynamics of the deep-trap PL that yield a time constant of $\sim 30 \text{ ps}$.³² In contrast to the time-resolved PL, the DT spectral maximum does not show any noticeable shift within several picoseconds after excitation. However, on a longer time scale ($\Delta t > 10 \text{ ps}$), the DT band starts to shift downward in energy until it finally reaches (at $\Delta t > 250 \text{ ps}$) the position of the cw PL maximum at 2.56 eV [see the normalized spectra in Fig. 1(b)]. This can be explained by the increasing relative contribution from the long-lived bleaching of the transition coupling the shallow hole trap to the lowest electron quantized state. At long delay times, after the electron state is completely depopulated, the bleaching of this transition is solely due to the trapped holes.

At pump levels above $\sim 0.5 \text{ mJ cm}^{-2}$, the DT dynamics begin to show a pump-intensity dependence (see the data from Sec. IV), indicating that we have reached the regime of the multiple e - h pair excitation, for which nonlinear decay processes start to play a significant role. The DT spectra

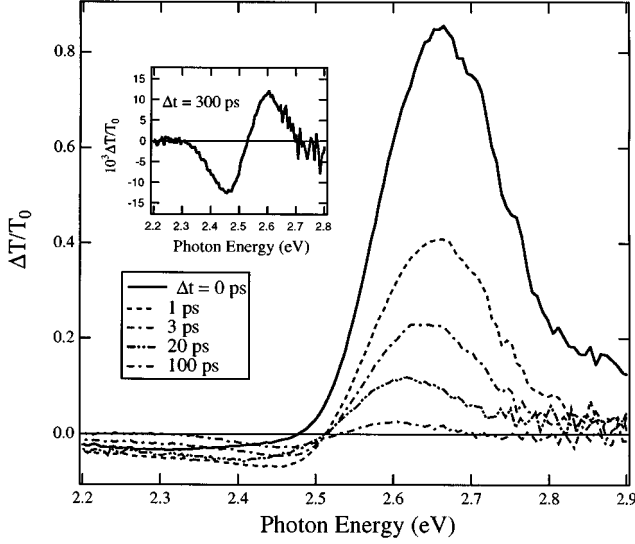


FIG. 2. DT spectra recorded at different delay times after excitation at a pump level $w_p = 10 \text{ mJ cm}^{-2}$, above the threshold for nonlinear recombination processes. The inset shows an expanded view of the spectrum measured at $\Delta t = 300 \text{ ps}$.

recorded in this regime are shown in Fig. 2. In contrast to the low-pump-intensity data, at high pump fluences, the bleaching maximum at 2.63 eV exhibits a much faster initial decay on the subpicosecond time scale. Another feature of the high-intensity DT is a new band of increased absorption located below the main bleaching band. The relative contribution from the induced absorption increases with increasing time delay until both features (bleaching and increased absorption) become essentially equivalent in magnitude (see the inset to Fig. 2). The shape of the DT spectra measured at high pump levels and at long times after excitation is drastically different from that measured at low pump fluences (see Fig. 3), although in both cases the average number of $e-h$ pairs per NC is well below one. Instead of a single bleaching band, the high-pump-intensity spectra show a derivativelike feature that is a clear signature of a dc electric-field-induced shift of the optical transition (dc Stark effect).²³ Similar transient absorption features were previously observed in NC's in the case of nonlinearities arising from carrier-trapping-induced charge separation²³ and the biexciton effect.²¹ The shape of DT at high pump fluences clearly indicates that the transition responsible for the nonlinearity couples unoccupied states (see the analysis of DT for competing contributions from the state filling and the transition shift in Ref. 21). The change in optical susceptibility $\Delta\chi(\omega)$ in this case can be described as

$$\Delta\chi(\omega) \propto \frac{\delta E}{(\hbar\Delta\omega + i\Gamma)(\hbar\Delta\omega + \delta E + i\Gamma)}, \quad (3.1)$$

where $\hbar\Delta\omega = \hbar\omega - E_0$, E_0 and Γ are the energy and the broadening of the optical transition, and δE is an electric-field-induced energy shift. The high-pump-intensity DT can be well fit (see Fig. 3) using the above formula with $E_0 = 2.546 \text{ eV}$, in agreement with the position of the positive band seen at long delay times in low-intensity DT spectra, which is attributed to the bleaching of the transition coupling

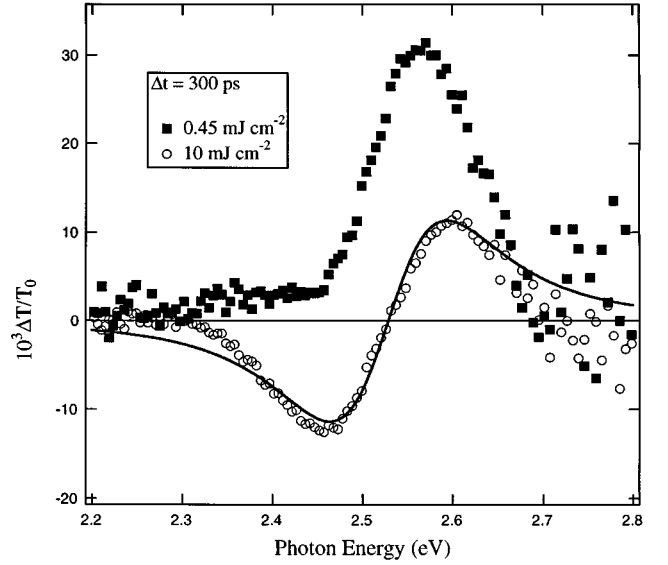


FIG. 3. Comparison of DT spectra recorded at 300 ps after excitation at low (solid squares) and high (open circles) pump intensities. A solid line shows the fit of the high-pump-intensity spectrum to a model spectrum calculated for a dc electric-field-induced shift of the optical transition centered at $E_0 = 2.546 \text{ eV}$ with broadening factor $\Gamma = 110 \text{ meV}$.

the occupied shallow hole trap to the unoccupied lowest electron quantized state. However, as is clear from the shape of the high-intensity DT spectra, the hole trap state is not occupied at high pump levels. This shows that the hole relaxation path changes at high pump fluences. Instead of being trapped at a shallow state with a relatively extended wave function, the hole most likely gets trapped at a state with much stronger localization. Due to the reduced overlap of the hole and the electron wave functions and/or a large low-energy shift of the corresponding transition (possibly below the observation range), this state is not marked by a pronounced feature in DT spectra. However, DT gets affected by new trapped states via the dc electric field generated as a result of the hole trapping. As the new hole relaxation channel is associated with an efficient charge separation, hole traps activated at high pump fluences are most likely surface/interface related. To clarify the mechanisms for the pump-intensity-dependent hole trapping, we performed accurate studies of the DT dynamics at different spectral energies in a wide pump-intensity range as discussed in the next section.

IV. PUMP-DEPENDENT DIFFERENTIAL-TRANSMISSION TIME TRANSIENTS

As a new hole relaxation path activated at high pump fluences is associated with the negative induced absorption feature below the main bleaching band, we have performed a careful comparison of dynamics measured at 2.4 eV (induced absorption) and 2.6 eV (bleaching). The corresponding time transients recorded at $w_p = 2.5 \text{ mJ cm}^{-2}$ (slightly above the threshold for observation of the induced absorption feature) are shown in Fig. 4, along with the pump-probe cross-correlation function. A simple analysis of these curves using the exponential decay (rise) function shows that the buildup of the signal at 2.4 eV is complementary to the decay of DT

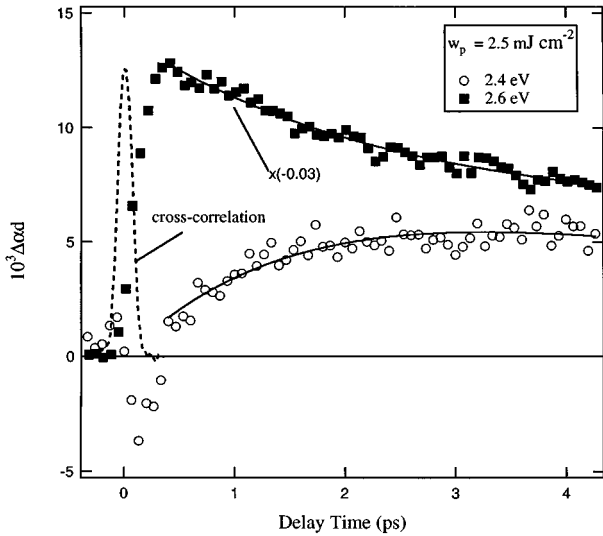


FIG. 4. Comparison of time evolution of DT recorded at 2.4 eV (increased absorption, open circles) and 2.6 eV (bleaching, solid squares) at $w_p = 2.5 \text{ mJ cm}^{-2}$ (thin solid lines show fits to exponential decay and buildup functions with a same time constant of 2.5 ps). The dashed line shows the pump-probe cross-correlation function.

at 2.6 eV; both are characterized by a time constant of 2.5 ps. The complementary behavior of the bleaching and the increased absorption is preserved at higher pump fluences (Fig. 5). Increasing the pump intensity leads to a faster decay of the bleaching band [Fig. 5(a)], which is accompanied by faster buildup dynamics of the induced absorption [Fig. 5(b)].

To understand a mechanism of a pump-dependent decay rate of the bleaching band and associated complementary buildup dynamics of the induced absorption feature, we have measured the pump-intensity dependence of DT at 2.4 and 2.6 eV at a fixed delay time ($\Delta t = 1 \text{ ps}$) between pump and probe pulses (Fig. 6). At pump levels below $\sim 2 \text{ mJ cm}^{-2}$, the bleaching increases almost linearly with pump intensity. A linear fit to the low-intensity data in the logarithmic plot gives a slope $p = 0.9$, as shown by the dashed line in Fig. 6. The induced absorption is characterized by a much steeper rise with initial slope of 3.1 (solid line in Fig. 6). At pump fluences above 2 mJ cm^{-2} , both curves show saturation. Interestingly, the bleaching signal saturates at a level $|\Delta\alpha/\alpha_0| \approx 0.7$, that is below the value of 1 that would be expected for a simple Fermi blocking of the transition with one unoccupied state. This shows that the observed saturation is caused by a mechanism different from Fermi blocking, as discussed below.

The complementary dynamics measured at 2.6 and 2.4 eV (Figs. 4 and 5) as well as the data on the pump dependences in Fig. 6 clearly indicate that the growth of induced absorption is associated with a cubic decay of the bleaching band. This type of nonlinear decay is a signature of Auger processes that previously have been reported as playing an important role in carrier recombination in highly excited NC's.^{27,33} The Auger decay involves three particles, two of which recombine, with the energy transfer to the third particle (an electron or a hole). The data from Sec. III show that this is a hole relaxation path that is different at high pump

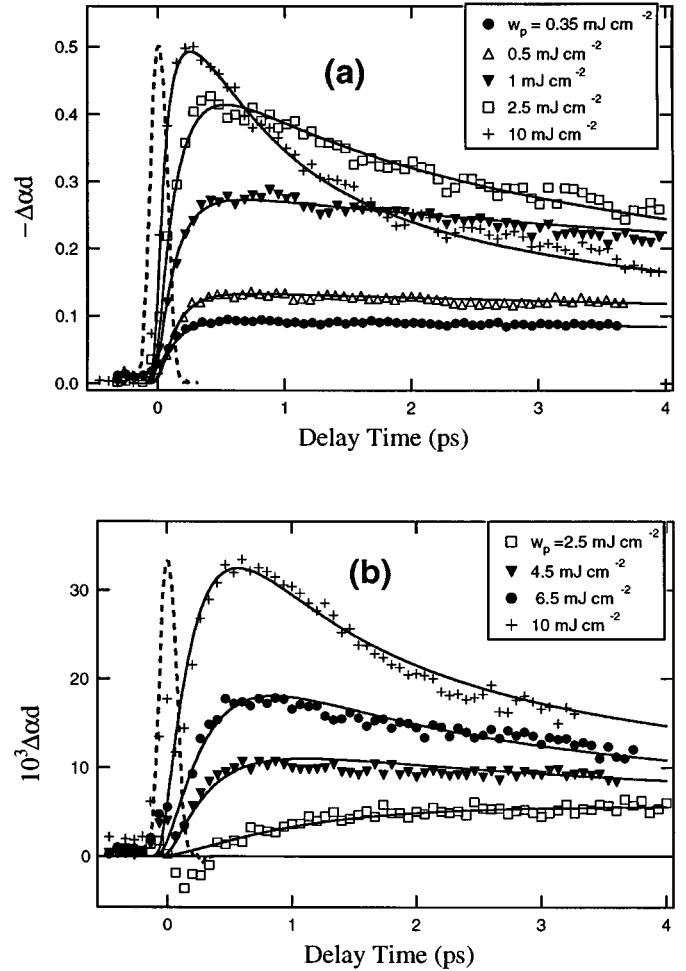


FIG. 5. Pump-dependent DT dynamics (symbols) recorded at (a) 2.6 eV (bleaching) and (b) 2.4 eV (increased absorption) along with fits (lines) calculated using a model of Auger-process-assisted trapping (see the text).

fluences. From this, we deduce that the Auger process plays the role of a reexcitation mechanism that promotes holes high enough in energy allowing them to overcome a NC-boundary-related potential barrier and to reach interface/surface-related states. Auger-assisted hole trapping at the surface leads to charge separation and the generation of strong local fields with the associated dc Stark shift seen in DT.

To gain a better understanding of the Auger-process-assisted surface trapping, we have developed a model schematically depicted in Fig. 7. Laser pumping leads to a generation of carriers in the excited quantized states; concentrations of these carriers are denoted as n_x^e (electrons) and n_x^h (holes). With a characteristic constant of $\tau_r^{e,h}$ (intra-band relaxation), the excited carriers relax to the lowest quantized states (corresponding carrier concentration are $n_l^{e,h}$). We include in the numerical model one type of trapping state for electrons (localization constant τ_l^e and concentration of the trapped electrons n_l^e) and two types of different hole trapping states. One type ($t1$ in Fig. 7) is active at low pump intensities and is accessible from the lowest hole quantized state (corresponding trapping constant τ_{t1}^h and concentration of the trapped holes n_{t1}^h). The other type of trapping

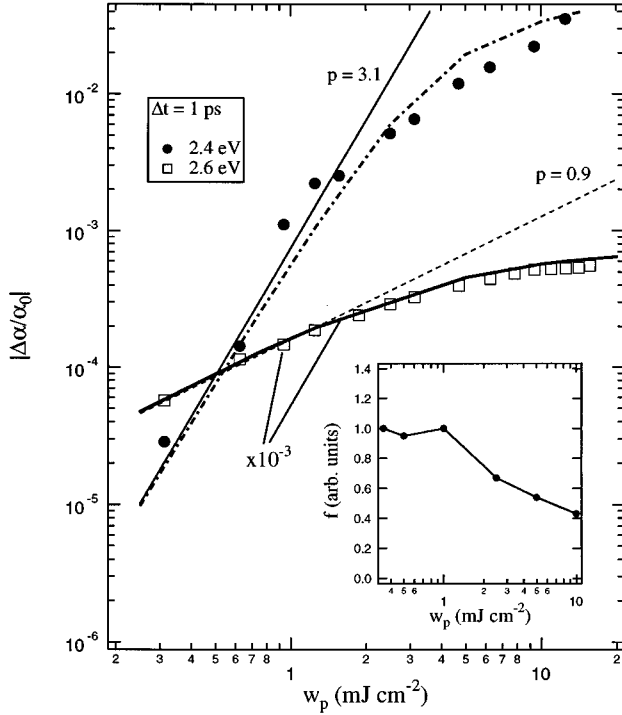


FIG. 6. Pump-intensity dependence of increased absorption at 2.4 eV (solid circles) and bleaching at 2.6 eV (open squares) measured at 1 ps after excitation in comparison with modeling results shown by thick solid and dash-dotted lines (see the text). Dashed and thin solid lines show pump-power dependences with logarithmic slopes 0.9 and 3.1, respectively. The inset shows the pump dependence of the oscillator strength of the lowest optical transition between quantized states derived by fitting experimentally measured DT dynamics at 2.6 eV.

states ($t2$), which are presumably surface/interface related, is separated from the hole quantized states by a potential barrier and can only be accessed after reexcitation. In our model, Auger-process-initiated reexcitation occurs via an intermediate hole excited state (denoted as rx in Fig. 7; corresponding concentration n_{rx}^h) from which holes relax to the $t2$ trapped state with a time constant τ_{t2}^h (concentration of the holes trapped at this type of states is n_{t2}^h). The essential point of the model is that all eight types of carriers occupying different NC states interact with each other via the Auger process. To describe the dynamics of photoexcited carriers in the above system, we have solved the following set of rate equations (only five equations for occupations of hole states are shown; the electron rate equations are similar to the first three from those given below):

$$\frac{dn_x^h}{dt} = g - \frac{n_x^h}{\tau_r^h} - n_x^h R_x^h, \quad (4.1)$$

$$\frac{dn_l^h}{dt} = \frac{n_x^h}{\tau_r^h} - \frac{n_l^h}{\tau_{t1}^h} - n_l^h R_l^h, \quad (4.2)$$

$$\frac{dn_{t1}^h}{dt} = \frac{n_l^h}{\tau_{t1}^h} - n_{t1}^h R_{t1}^h, \quad (4.3)$$

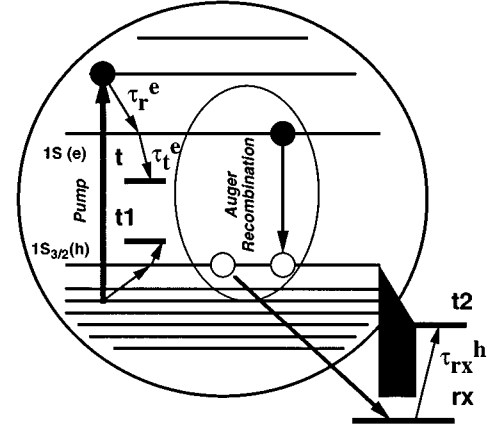


FIG. 7. Schematic diagram illustrating the model of Auger-process-assisted hole trapping at surface/interface states. Laser pumping results in a population of the excited electron (hole) quantized states in a NC. With relaxation constants $\tau_r^{e,h}$ carriers relax to the lowest quantized states [$1S(e)$ and $1S_{3/2}(h)$]. From these states carriers can be trapped at t (electrons) or $t1$ (holes) localized states. Because of the potential barrier at a NC boundary, the hole trapping at the $t2$ surface/interface-related state can only occur after reexcitation via an Auger process.

$$\frac{dn_{rx}^h}{dt} = \frac{1}{2} (n_x^h R_x^h + n_l^h R_l^h + n_{t1}^h R_{t1}^h) - \frac{n_{rx}^h}{\tau_{rx}^h} - n_{rx}^h R_{rx}^h, \quad (4.4)$$

$$\frac{dn_{t2}^h}{dt} = \frac{n_{rx}^h}{\tau_{rx}^h} - n_{t2}^h R_{t2}^h, \quad (4.5)$$

where g is the pumping rate; $R_i^l = \sum_{j,k,m,n} C_{ijk}^{lmn} n_j^m n_k^n$ is the Auger recombination term; C_{ijk}^{lmn} are the Auger constants; l, m, n indicate either electron (e) or hole (h) states [one of the carriers in the (l, m, n) combination is necessarily different from the other two]; and i, j, k denote the type of these states (x, l, t for electrons and $x, l, t1, rx, t2$ for holes). As we are mostly interested in early picosecond dynamics, we neglect the slow linear relaxation of the trapped states. Assuming a dominant role of the state filling in the 2.6-eV bleaching (with a principal contribution from the electrons; see the discussion in Sec. III), we model $\Delta\alpha$ ($\hbar\omega = 2.6$ eV) as proportional to n_l^e : $\Delta\alpha \propto f n_l^e$, where f is the oscillator strength of the corresponding optical transition (the contribution from the transition energy shift to the bleaching band is negligibly small on the time scale shown in Figs. 4 and 5). As the pump-induced absorption at 2.4 eV is associated with the dc electric field induced by the surface-trapped holes, we assume that this signal is proportional to n_{t2}^h .

We start a fitting procedure with the low-intensity data that are not affected by the Auger recombination. By fitting the rise and decay times of DT at 2.6 eV we derive the electron intraband relaxation constant ($\tau_r^e = 140$ fs) and the electron trapping time ($\tau_t^e = 35$ ps). As the initial hole relaxation at low pump levels is almost “invisible” in DT, we assume arbitrary that $\tau_r^e = \tau_r^h$ and use the value of 1 ps for τ_{t1}^h based on the PL dynamics from Ref. 25. To simplify the fit to the high-pump-intensity data, we assume that the Auger constants can have only one of two values: C_b for recombination terms that do not involve surface/interface states (rx

or t_2) and C_i for all other Auger terms in rate equations (4.1)–(4.5). As the relatively slow buildup of the induced absorption at pump intensities around 2.5 mJ cm^{-2} (the threshold for generation of the increased absorption feature) is dominated by the Auger processes, we fit these data to find a value of the C_b constant: $C_b^{-1}V_0^2 = 5.5 \text{ ps}$ (V_0 is a volume of a single NC). At higher pump intensities, the buildup dynamics of the 2.4-eV feature start to be sensitive to the τ_{rx} relaxation constant, which allows us to derive a value of 200 fs for it. Finally, the fits to decay dynamics of increased absorption and bleaching at high pump intensities give us the value of the C_i constant: $C_i^{-1}V_0^2 = 1.8 \text{ ps}$.

Now we address a peculiarity in the behavior of the bleaching time transients observed at high intensities and manifested as intersections of traces recorded at different pump fluences [see Fig. 5(a)]. This effect is entirely reversible and therefore cannot be attributed to a sample degradation (photodarkening).³⁴ However, this behavior cannot be described by the proposed model without an additional assumption about the pump-dependent oscillator strength of the optical transition at 2.6 eV. To fit accurately not only dynamics but also the magnitude of the bleaching, we have assumed that at high pump levels (above $\sim 1 \text{ mJ cm}^{-2}$) the oscillator strength starts to decrease with increasing pump intensity. This can be attributed to the influence of the electric field generated as a result of the hole surface trapping, leading to a modification of the symmetry of the electron and hole wave functions.¹⁵ By fitting the amplitudes of time transients recorded at different pump intensities we were able to derive the pump dependence of the oscillator strength shown in the inset to Fig. 6. Using a single set of relaxation parameters derived in a stepwise manner, as discussed above, and introducing the variable oscillator strength (see the inset to Fig. 6), we were able to fit excellently all dynamics recorded at both 2.4 and 2.6 eV over a wide pump intensity range [see Figs. 5(a) and 5(b)].

The validity of the above model has been verified by applying it to describe the pump-intensity dependences shown in Fig. 6. In the calculations we have used the same set of relaxation parameters and the same pump dependence of the

oscillator strength as those derived by fitting the time transients. In Fig. 6 we show the solutions of the rate equations for the bleaching (proportional to n_i^e ; thick solid line) and increased absorption (proportional to n_i^h ; dash-dotted line) at 1 ps after excitation as a function of a pump fluence. As seen from this figure, the model explains very well not only the slopes measured for the bleaching ($p \approx 1$) and the increased absorption ($p \approx 3$) at low pump levels but also the saturation of both at high pump intensities. This shows that the saturation observed experimentally occurs entirely due to the Auger recombination that effectively limits the occupation of the lowest quantized states at a level below the threshold for the Fermi blocking.

V. CONCLUSION

We have performed careful studies of femtosecond transient absorption in CdS NC's over a wide pump intensity range, starting from levels where the average number of e - h pairs per NC is less than one and up to levels where nonlinear recombination processes play a significant role. We have observed a strong difference in nonlinear optical response at low and high pump intensities, indicating a change in the dominant hole relaxation channel as a result of nonlinear interactions in the system of photoexcited carriers. The nonlinear transmission measured at high pump fluences has a clear signature of a dc electric-field-induced Stark shift of optical transitions, indicative of charge separation due to carrier surface trapping. A careful analysis of the nonlinear transmission time transients and pump dependences shows that this charge separation is caused by the third-order Auger process acting as a reexcitation mechanism that promotes holes high enough in energy to allow them to overcome the NC-boundary-related potential barrier and to reach the interface/surface-related states.

ACKNOWLEDGMENT

This research was supported by Los Alamos Directed Research and Development funds, under the auspices of the U.S. Department of Energy.

*Mailing address: CST-6, MS-J585, Los Alamos National Laboratory, Los Alamos, NM 87545. Electronic address: klimov@lanl.gov

¹A. P. Alivisatos, *Science* **271**, 933 (1996).

²H. Weller, *Angew. Chem. Int. Ed. Engl.* **32**, 41 (1993).

³V. S. Dneprovskii, V. I. Klimov, D. K. Okorokov, and Yu. V. Vandyshv, *Solid State Commun.* **81**, 227 (1992).

⁴V. Colvin, M. C. Schlaman, and A. P. Alivisatos, *Nature* **370**, 354 (1994).

⁵A. Sergio Bezerra Sombra, *Solid State Commun.* **88**, 305 (1993).

⁶A. Hagfeld and M. Graetzel, *Chem. Rev.* **95**, 49 (1995).

⁷C. B. Murray, D. J. Norris, and M. G. Bawendi, *J. Am. Chem. Soc.* **115**, 8706 (1993).

⁸M. Nogami, S. Suzuki, and K. Nagasava, *J. Am. Ceram. Soc.* **75**, 220 (1992).

⁹Al. L. Efros and A. L. Efros, *Fiz. Tekh. Poluprovodn.* **16**, 1209 (1982) [*Sov. Phys. Semicond.* **16**, 772 (1982)].

¹⁰Y. Z. Hu, S. W. Koch, and D. B. Tran Thoai, *Mod. Phys. Lett.* **4B**, 1009 (1990).

¹¹L. Banyai, P. Gilliot, Y. Z. Hu, and S. W. Koch, *Phys. Rev. B* **45**, 14 136 (1992).

¹²L. E. Brus, *J. Chem. Phys.* **80**, 4473 (1984).

¹³Al. L. Efros and A.V. Rodina, *Solid State Commun.* **72**, 645 (1989).

¹⁴S. W. Koch, Y. Z. Hu, B. Fluegel, and N. Peyghambarian, *J. Cryst. Growth* **117**, 592 (1992).

¹⁵Y. Z. Hu, M. Lindberg, and S. W. Koch, *Phys. Rev. B* **42**, 1713 (1990).

¹⁶S. Nomura and T. Kobayashi, *Solid State Commun* **78**, 677 (1991).

¹⁷A. I. Ekimov, F. Hache, M. C. Schanne-Klein, D. Ricard, C. Flytzanis, I. A. Kudryavtsev, T. V. Yazeva, A. V. Rodina, and Al. L. Efros, *J. Opt. Soc. Am. B* **10**, 100 (1993).

¹⁸J.-B. Xia, *Phys. Rev. B* **40**, 8500 (1989).

¹⁹B. Fluegel, M. Joffre, S. H. Park, R. Morgan, Y. Z. Hu, M. Lindberg, S. W. Koch, D. Hulin, A. Migus, A. Antonetti, and N. Peyghambarian, *J. Cryst. Growth* **101**, 643 (1990).

- ²⁰V. Klimov, S. Hunsche, and H. Kurz, *Phys. Status Solidi B* **188**, 259 (1995).
- ²¹V. Klimov, S. Hunsche, and H. Kurz, *Phys. Rev. B* **50**, 8110 (1994).
- ²²K. I. Kang, A. D. Kepner, S. V. Gaponenko, S. W. Koch, Y. Z. Hu, and N. Peyghambarian, *Phys. Rev. B* **48**, 15 449 (1993).
- ²³D. J. Norris, A. Sacra, C. B. Murray, and M. G. Bawendi, *Phys. Rev. Lett.* **72**, 2612 (1994).
- ²⁴V. Milanović and Z. Ikonić, *Phys. Rev. B* **39**, 7982 (1989).
- ²⁵V. Klimov, P. Haring-Bolivar, and H. Kurz, *Phys. Rev. B* **53**, 1463 (1996).
- ²⁶M. C. Nuss, W. Zinth, and W. Kaiser, *Appl. Phys. Lett.* **49**, 1717 (1986).
- ²⁷J. Z. Zhang, R. H. O'Neil, and T. W. Roberti, *Appl. Phys. Lett.* **64**, 1989 (1994).
- ²⁸V. Klimov, P. Haring-Bolivar, H. Kurz, and V. Karavanskii, *Superlatt. Microstruct.* **20**, 395 (1996).
- ²⁹N. F. Borelli, D. W. Hall, H. J. Holland, and D. W. Smith, *J. Appl. Phys.* **61**, 5399 (1987).
- ³⁰V. Klimov and V. Karavanskii, *Phys. Rev. B* **54**, 8087 (1996).
- ³¹S. Hunsche, T. Dekorsy, V. Klimov, and H. Kurz, *Appl. Phys. B* **62**, 3 (1996).
- ³²M. O'Neil, J. Marohn, and G. McLendon, *Chem. Phys. Lett.* **168**, 208 (1990).
- ³³M. Ghanassi, M. C. Schanne-Klein, F. Hache, A. I. Ekimov, D. Ricard, and C. Flytzanis, *Appl. Phys. Lett.* **62**, 78 (1993).
- ³⁴M. Tomita and M. Matsuoka, *J. Opt. Soc. Am. B* **7**, 1198 (1990).